Journal of Materials Science: Materials in Electronics (2019) 30:12783–12789
https://doi.org/10.1007/s10854-019-01643-z

Structural, superconducting and vortex pinning properties of Nb-substituted Bi-2212 ceramic superconductor

F. Karaçora Nane[1] · B. Özçelik[2]

Received: 22 January 2019 / Accepted: 3 June 2019 / Published online: 8 June 2019
© Springer Science+Business Media, LLC, part of Springer Nature 2019

Abstract
In this research, we have deeply focused to investigate the effects of Niobium (Nb) substitution for the Ca site in the $Bi_2Sr_2Ca_{1-x}Nb_xCu_2O_{8+y}$ superconductors with x = 0.00, 0.05, 0.10, 0.20, 0.30, and 0.40. The materials were synthesized via well-known solid state reaction method. We have performed X-ray diffraction (XRD), scanning electron microscopy (SEM), energy dispersive X-ray spectroscopy (EDX), and dc magnetization measurements in order to understand the effects of Nb-content. XRD results exhibit that the Bi-2212 phase is a major phase for pure sample. On the other hand, the volume fraction of Bi-2212 declines with increasing Nb substitution and relocates with low-*Tc* phase, namely Bi-2201. The maximum pinning force, F_{Pmax}, values of x = 0.05 and 0.10 Nb-substituted samples are improved in comparison to the pure sample. These values are found as 5.18×10^7 and 5.21×10^7 Oe A/cm^2 at T = 10 K for x = 0.05 and 0.10 Nb-substituted sample, respectively, which are higher than the 4.92×10^7 Oe A/cm^2 value of the pure sample.

1 Introduction

Shortly after the discovery of superconductivity was found in the bismuth family by Michel et al. [1, 2], Maeda reported in a subsequent study that the first cuprate family without rare earth elements have a Tc of over 110 K. [3]. Bi-based superconductor family has three members given a formula of $Bi_2Sr_2Ca_{n-1}Cu_nO_x$ where $n = 1, 2, 3$. The critical temperatures of Bi-2201, Bi-2212 and Bi-2223 phases are around 20, 85, and 110 K, respectively. The production of superconducting materials in a single phase is vital for potential industrial applications. The Bi-2212 phase with *Tc* value of 85 K which is above liquid nitrogen and has better stability comparison to Bi-2223 phase, is the most popular phase for possible applications such as tapes, superconducting wires, and thin films [4, 5]. In recent years, experimentalist have tried to improve the physical and superconducting properties of BSCCO system by using several methods [6–13]. Especially, one of the most useful methods to improve the physical properties is the substitution of some elements at different cationic sites. As it is well-known, these substitutions cause very important variations in the carrier concentration and also remove the restriction of spin alignment arising from the spin lattice interaction [14]. These important variations support to understanding the microstructural and superconducting properties along with the physical mechanism of superconductivity [15–17]. In addition to chemical doping, the synthetic methods have been extensively investigated by scientists to produce homogeneous and high quality samples. The Bi-based superconductors can be produced via conventional solid state technique [18] or with other routes such as sol–gel [19], and polymerization techniques [20]. These wet routes are focus on producing Bi-based superconductor powders with high purity and homogeneity. Finally, conventional solid state technique is still hot topic based on trying to produce bulk ceramic superconductors with better optimum conditions of doping, substituting and producing process.

In previous works, in order to obtain pure Bi-2223 phase high valency cations like Nb, Ti and V for Cu substituted have been studied [21, 22]. The purposes of this study are: (i) determining optimum contents of Nb into the Ca site of $Bi_2Sr_2Ca_{1-x}Nb_xCu_2O_{8+y}$ system, (ii) exploring the micro structure and magnetic properties of the substituted systems (iii) evaluating the results depending on Nb content. Therefore, in this research, the variations of superconducting properties

✉ B. Özçelik
ozcelik@cu.edu.tr

[1] Department of Electrical and Electronic Engineering, Faculty of Engineering, Hakkari University, 30000 Hakkari, Turkey

[2] Department of Physics, Faculty of Sciences and Letters, Çukurova University, 01330 Adana, Turkey

induced from the Nb substitution for Ca have been deeply investigated via X-ray diffraction (XRD), scanning electron microscopy (SEM), electron dispersive X-ray (EDX), dc-magnetization and magnetic hysteresis techniques.

2 Experimental details

$Bi_2Sr_2Ca_{1-x}Nb_xCu_2O_y$ bulk ceramics (x = 0.00, 0.05, 0.10, 0.20, 0.30, and 0.40) were produced by well-known solid state reaction from the commercial powders of Bi_2O_3 (Sigma-Aldrich, 99.9%), $SrCO_3$ (Sigma-Aldrich, 98 + %), $CaCO_3$ (Sigma-Aldrich, ≥ 99%), Nb_2O_5 (Sigma-Aldrich, 98 + %), and CuO (Sigma-Aldrich, 99%). The powders were firstly weighed in the appropriate proportions, and then mixed and milled in an agate mortar. For calcination, two steps heat treatment was performed on powders at 750 and 800 °C for 24 h with an intermediate manual milling. Finally, the prereacted homogeneous powders were pressed into pellets with 13 mm in diameter by applying a pressure of 350 MPa. On the other hand, as it is well-known, Bi-2212 ceramics show the presence of several secondary phases formed by their characteristic incongruent melting. As a consequence, a thermal treatment is necessary to obtain the superconducting phase after the calcination process. This annealing process was performed in a tubular furnace under air atmosphere and consisted in two steps: 60 h at 860 °C in order to form the Bi-2212 phase, followed by 12 h at 800 °C to adjust the oxygen content and, finally, quenched in air to room temperature.

In order to identify the present phases, powder X-ray diffraction patterns of the samples were measured at room temperature using a Rigaku D/max-B powder diffractometer system working with CuKα radiation and a constant scan rate between 2θ = 5°–80°. The uncertainty of the crystal lattice parameters calculation remained in the ± 0.0001 range. By using the least squares method, the lattice parameters of all samples were calculated from *d* values and (*hkl*) parameters. SEM micrographs of all samples were taken using a LEO Evo-40 VPX scanning electron microscope (SEM) fitted with an energy dispersive x-ray spectroscopy (EDX) analysis system. All SEM micrographs have been taken from backscattered mode from transversal sections. The magnetic hysteresis measurements of samples were performed at 10, 15 and 20 K under ± 10 kOe applied field, and *M(T)* measurement was obtained under 50 Oe applied field in ZFC mode with a 7304 model Lake Shore VSM.

3 Results and discussion

3.1 XRD characterization

In Fig. 1, the normalized powder XRD patterns are displayed. This graph exhibits that the major phase in pure sample is Bi-2212 one. By increasing Nb-content, the volume fraction of Bi-2201 phase is starting gradually to increase. Besides, small amounts of $CuNb_2O_6$ (labeled by **o**) non-superconducting phase (ICSD Catalog Number: 01-083-0369) were detected after 0.10Nb content. The crystal symmetry of all samples was determined as pseudo tetragonal. The lattice parameters were calculated by using the least squares method and tabulated in Table 1.

For obtaining more information about the crystal structure, we have used the Debye Scherer formula [23] given as:

$$L_{hkl} = \frac{0.9\,\lambda}{\beta \cos\theta} \quad (1)$$

where λ is wavelength, β is the full width at half maximum and θ is the angle of the peak. The maximum average crystal size was found as 407 Å for 0.20Nb substituted sample. All these data are in agreement with the literature found for different substitutions [24, 25].

3.2 SEM and EDX analysis

Figure 2 shows the surface morphologies of all bulk samples consisting of typical grains of BSCCO system, align randomly. It can clearly be seen that after 0.10Nb substitution, the general structure has composed by oriented grains along *a-b* plane due to partial melting caused by more amount of Nb. In addition, some sand-like regions have observed in main matrix of 0.30Nb and 0.40Nb substituted samples. According to EDX results of 0.40Nb sample displayed in Fig. 3, these structures correspond to the Sr + Nb rich phase.

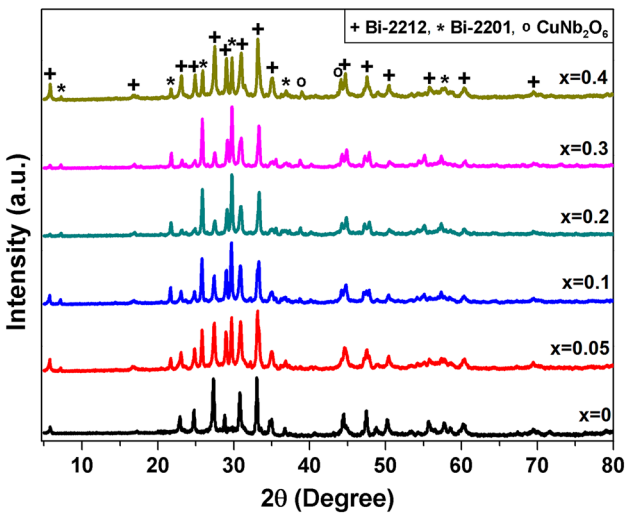

Fig. 1 XRD patterns of the all samples. Peaks corresponding to the Bi-2212, Bi-2201, and $CuNb_2O_6$ phases are indicated by plus, asterisk, and open circle respectively

Table 1 T_c values deduced from the dc *M–T* measurement data, unit cell parameters, crystal size and maximum pinning force of samples

Concentration *x*	T_c (K)	Unit-cell parameter $a=b$ (Å)	Unit-cell parameter *c* (Å)	Crystal size L_{hkl} (Å)	F_{pmax} at 10 K (Oe A/cm^2) 10^7
$x=0.00$	83.8	5.4180	30.8028	365	4.92
$x=0.05$	83.8	5.3990	30.7587	346	5.18
$x=0.10$	83.4	5.3830	30.8150	374	5.21
$x=0.20$	81.3	5.3705	30.8183	407	3.06
$x=0.30$	78.8	5.3736	30.7160	398	2.16
$x=0.40$	76.0	5.3925	30.8245	346	1.59

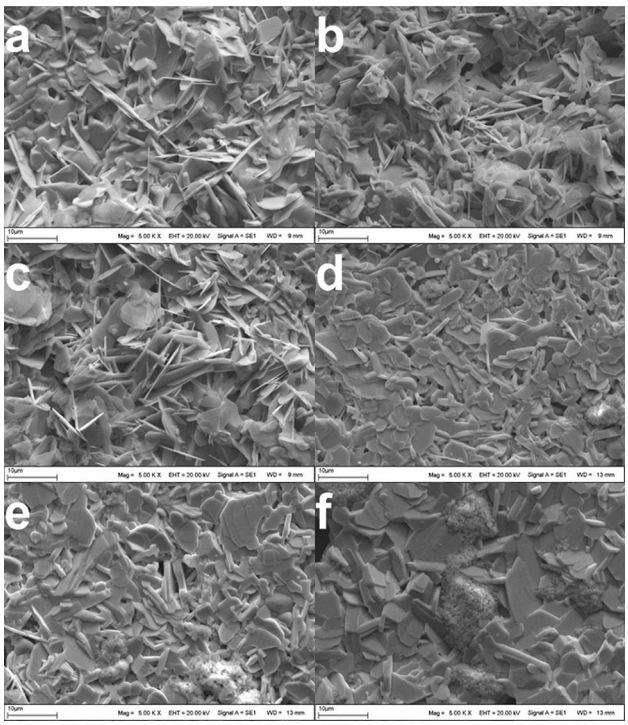

Fig. 2 SEM micrographs of the $Bi_2Sr_2Ca_{1-x}Nb_xCu_2O_y$ samples with x = **a** 0.00, **b** 0.05, **c** 0.10, **d** 0.20, **e** 0.30, and **f** 0.40

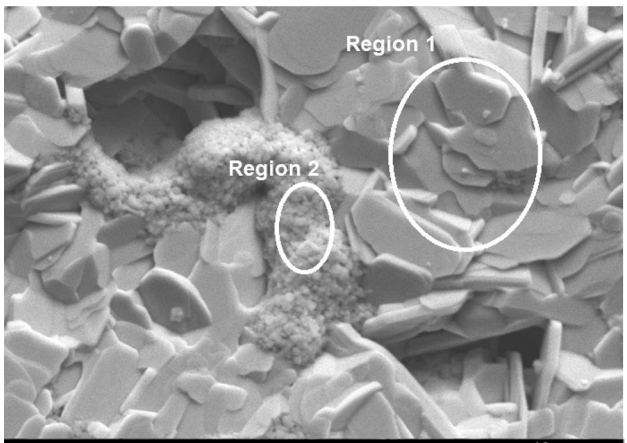

Selected Region for EDX	Bi	Sr	Ca	Cu	Nb
Region 1	2.1	1.6	1.2	1.9	0.2
Region 2	0.6	3.4	1.3	0.2	1.5

Fig. 3 SEM micrograph and EDX results performed on $Bi_2Sr_2Ca_{0.6}Nb_{0.4}Cu_2O_y$ (x = 0.40) sample

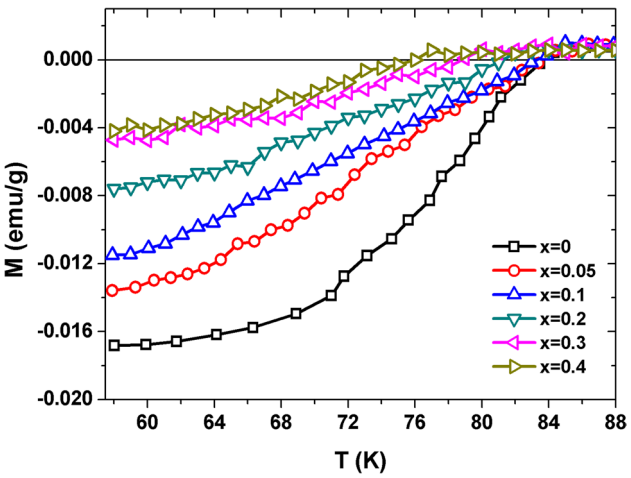

Fig. 4 Magnetization versus temperature for the different Nb-content

3.3 Magnetic properties

The temperature dependence of zero field cooled (ZFC) magnetization which gives intragrain *Tc* values with the currents circulating inside the grains due to the weak links between grains was obtained for all samples and exhibited in Fig. 4. The *M-T* data show that pure and 0.05Nb substituted sample have a same T_C value of 83.8 K, and then the critical transition temperature decreases with increasing of Nb content. This lowering in transition temperature arises from increasing in volume fraction of Bi- 2201 phase as seen in XRD data causing by more Nb content.

The initial (virgin) curves of dc magnetizations versus magnetic fields, between 0 and 10 kOe, at 10 K have been measured and given in Fig. 5. Such a kind of experiment is very

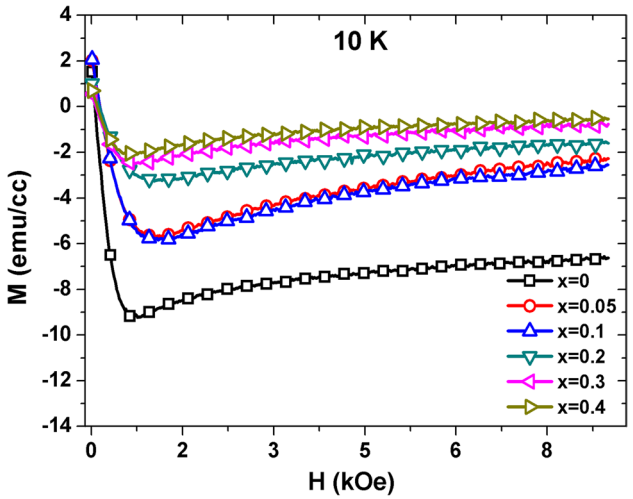

Fig. 5 Magnetization versus applied field (initial curve) for the different Nb-content

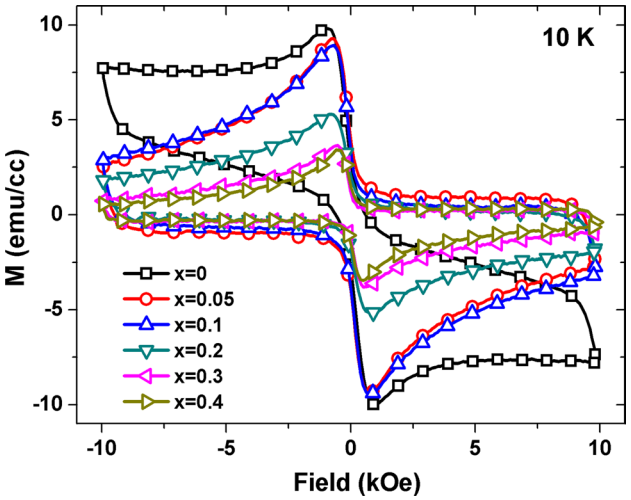

Fig. 6 *M–H* loops for all samples measured at 10 K

attractive tool to obtain more information about Meissner and vortex regions divided by the critical applied field H_{C1}. The applied field values below and above H_{C1} mean Meissner and Abrikosov vortex regions, respectively. H_{C1} values of 0.05, 0.10, and 0.20Nb substituted samples, exhibited in Fig. 5 are relatively higher than pure sample, except for 0.30 and 0.40Nb substitutions. The highest H_{C1} value was found as 1185 Oe for 0.10Nb sample.

The magnetic hysteresis loops of all samples were obtained at 10 K between applied fields of ± 10 kOe and are shown in Fig. 6. These hysteresis curves show that the 0.05 and 0.10Nb substituted samples have wider loops than pure sample implying an improved intragranular structure induced by Nb. After 0.10Nb content, the hysteresis loops get gradually narrow for higher Nb-content. In addition, an extended measurement was performed on 0.05 and 0.10Nb samples in order to obtain the temperature dependent hysteresis loops at 10, 15, and 20 K. The results are given in Fig. 7. It can be seen that the applied field penetration becomes difficult due to the pinning effect at 10 K, later on the applied field begins to permeate into intragranular texture of materials with increasing temperature resulting in thermally activated flux flow (TAFF) effect.

3.4 Critical current density calculation

From magnetic hysteresis loops, the intragranular critical current density *Jc* values of the samples were calculated using the Bean's model [26];

$$J_c = \frac{60a|\Delta M|}{b(3a-b)} \quad (2)$$

where J_C is known as the critical current density in Ampéres per square centimeter of a sample. $\Delta M = M_+ - M_-$ is measured in electromagnetic units per cubic centimeter, a and b are the length of the sample plane perpendicular to the applied magnetic field. By using *M–H* loops, the calculated magnetic critical current density (*Jc*) values are plotted in Fig. 8. According to comparable J_C values, Nb substitution to Bi- 2212 phase does not make significant change on pinning mechanism resisting the flux creep. Only x = 0.05 and 0.10 Nb-substituted samples have shown better performance than pure samples. But the field dependence of these samples is seen to be higher than pure one's. The maximum critical current density was calculated as 1.7×10^4 A/cm^2 for x = 0.05 sample. This value is almost at the same magnitude with the Vanadium substituted sample [25], but it is lower than the samples prepared different routes [13, 24].

3.5 Pinning mechanism

To understand the nature of vortex pinning mechanism, the pinning forces were calculated by using $F_P = Jc \times \mu\mu_0 H$ equation [27]. For all samples, at 10 K, the calculated pinning force, $F_P(H)$, values were presented in Fig. 9a, and maximum pinning force values tabulated in Table 1. In general, the calculated pinning force value increased rapidly for low applied magnetic field values, and then it decreases suddenly after magnetic field of 9 kOe for all samples. The F_{Pmax} values of 0.05 and 0.10Nb substituted samples are higher than the value of pure sample. The maximum pinning force was calculated as 5.21×10^7 Oe A/cm^2 for 0.10Nb sample. This value is slightly the same with the maximum pinning force calculated for 0.05 V sample [25]. The reduced pinning force F_P/F_{Pmax} versus reduced magnetic field B/B_{irr} is given in Fig. 9b. The same behavior of all samples indicated

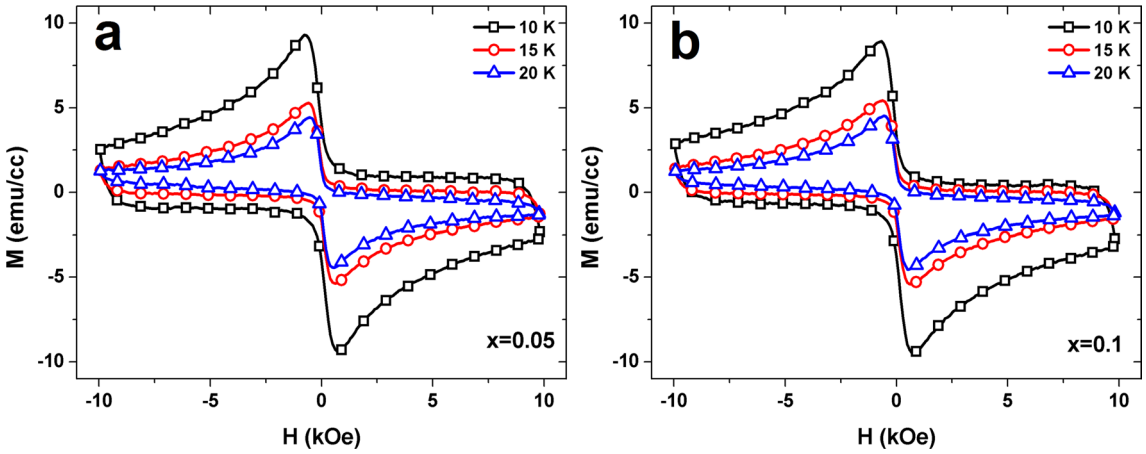

Fig. 7 *M–H* loops at 10, 15, and 20 K for the sample: **a** x = 0.05, **b** x = 0.10

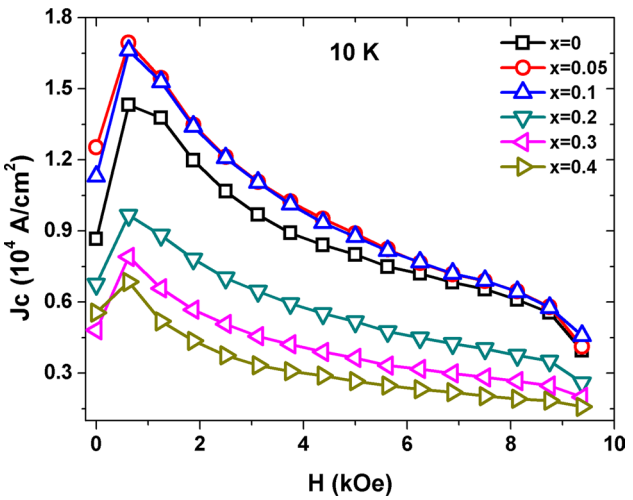

Fig. 8 Calculated critical current densities, J_c, of the samples, as a function of the applied magnetic field, at 10 K

that a kind of vortex pinning mechanism is identical for all samples. Moreover, comparative F_P versus B and F_P/F_{Pmax} versus B/B_{irr} results of 0.05 and 0.10Nb substituted samples for different temperature were given in Fig. 10. For both samples, pinning force value decreases with increasing of temperature from 10 to 20 K. Furthermore, F_{Pmax} values of these samples have decreased by around 75% due to the thermally activated flux flow (TAFF) effect.

4 Conclusions

In this study, $Bi_2Sr_2Ca_{1-x}Nb_xCu_2O_{8+y}$ bulk ceramics with x = 0.00, 0.05, 0.10, 0.20, 0.30, and 0.40 were synthesized by using well-known classical solid state method and investigated by XRD, SEM, *M–T, M–H* J_C*–H* and estimated vortex pinning force to obtain the optimum substitution value of niobium. The results have indicated

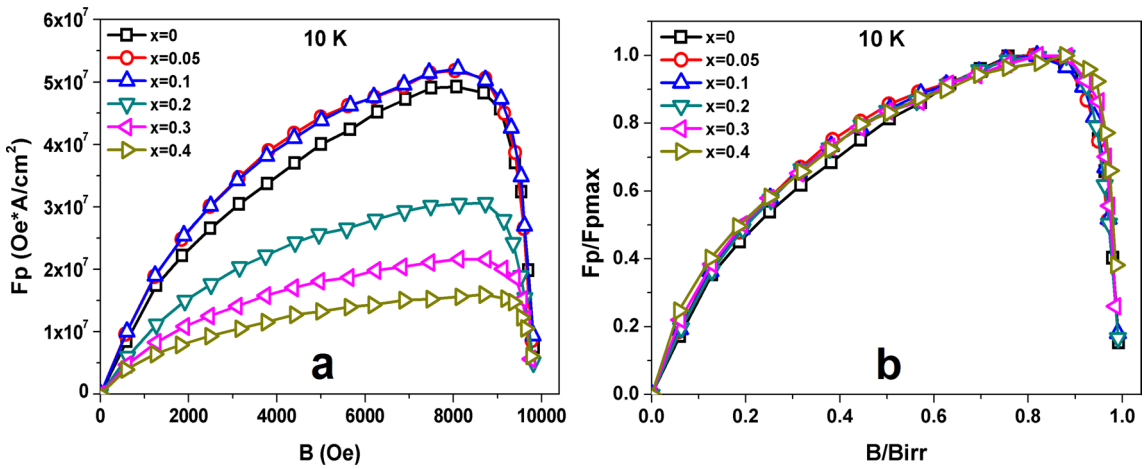

Fig. 9 **a** Pinning force versus applied field. **b** Reduced pinning force versus reduced applied field, for the different Nb-content, at 10 K

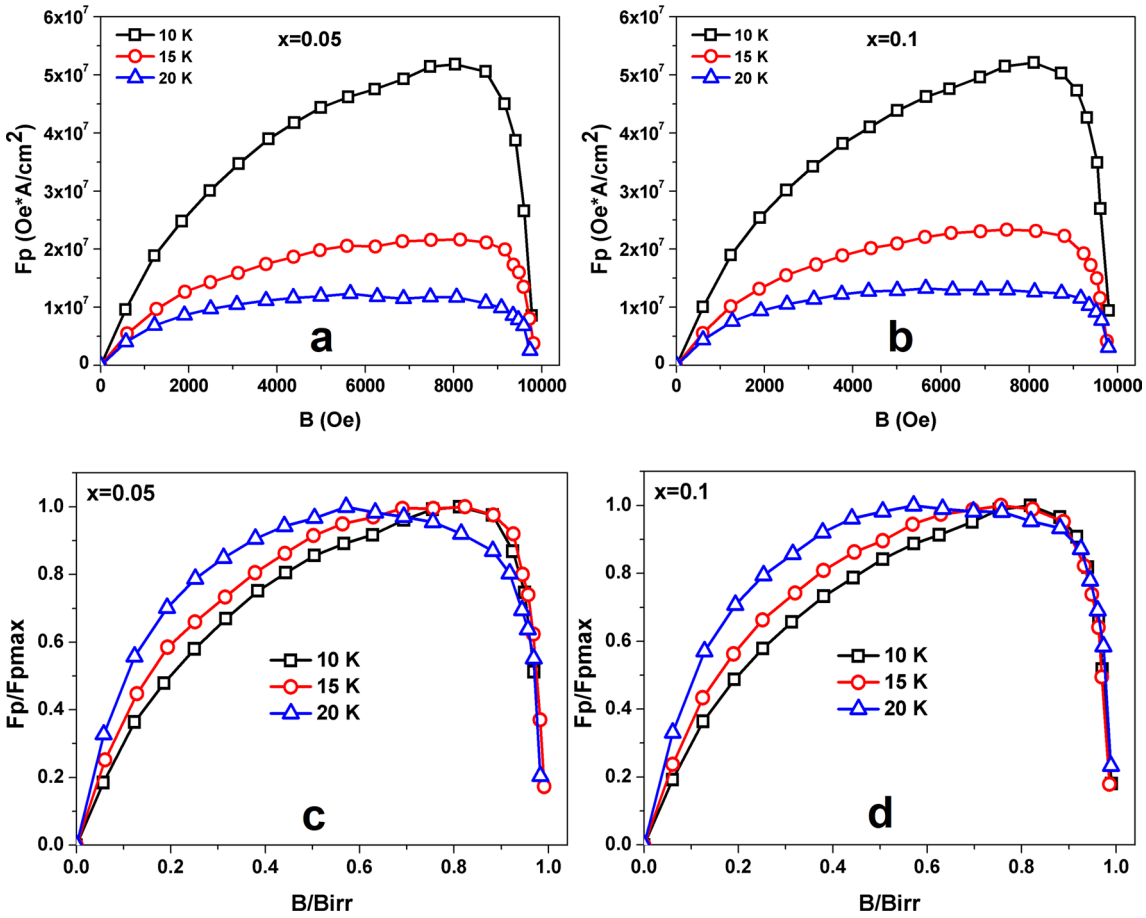

Fig. 10 **a** Pinning force versus applied field for x = 0.05. **b** Pinning force versus applied field for x = 0.10. **c** Reduced pinning force *F/Fpmax* versus reduced applied field *H/Hmax* for x = 0.05. **d** Reduced pinning force *F/Fpmax* versus reduced applied field *H/Hmax* for x = 0.10, at 10, 15, and 20 K

that Nb substitution have not significantly modified the superconducting properties of samples, while structural decomposition has increased with more Nb content. It has been found that the increase on Nb content has produced an increment of *Jc* values up to x = 0.1Nb by employing the critical Bean model. The maximum critical current density has been calculated as 1.7×10^4 A/cm^2 for x = 0.05 and 0.10 samples. The pinning mechanism by using experimental data has also theoretically investigated. The results have indicated that the pinning centers in the all samples present a normal point pinning nature and the maximum pinning force has been calculated as 5.21×10^7 Oe A/cm^2 for 0.10Nb sample. All these results clearly point out the effect of high temperatures, under air, on the ability of Nb to raise physical properties.

Finally, it may be argued that we have observed a significant improvement in J_C and F_{Pmax} values of 0.05Nb and 0.10Nb samples.

References

1. C. Michel, M. Hervieu, M. Borel, A. Grandin, F. Deslandes, J. Provost, B. Raveau, Z. Phys. B **68**, 421 (1987)
2. H.G. von Schnering, L. Walz, M. Schwarz, W. Becker, M. Hartweg, T. Popp, B. Hettich, P. Müller, G. Kämpf, Angew. Chem. Int. Ed. Engl. **27**, 574–576 (1988)
3. H. Maeda, Y. Tanaka, M. Fukutomi, T. Asano, Jpn. J. Appl. Phys. **27**, L209 (1988)
4. O. Nane, B. Özçelik, D. Abukay, J. Alloy Compd. **566**, 175 (2013)
5. O. Nane, B. Özçelik, D. Abukay, Ceram. Int. **42**(5), 5778 (2016)
6. M. Mora, A. Sotelo, H. Amaveda, M.A. Madre, J.C. Diez, L.A. Angurel, G.F. de la Fuente, Bol. Soc. Esp. Ceram. **44**, 199 (2005)
7. M. Zargar Shoushtari, S.E. Mousavi Ghahfarokhi, J. Supercond. Nov. Magn. **24**, 1505 (2011)
8. A.I. Abou-Aly, M.M.H. Gawad, I. G-Eldeen, J. Supercond. Nov. Magn. **24**, 2077 (2011)
9. M. Mora, A. Sotelo, H. Amaveda, M.A. Madre, J.C. Diez, L.A. Angurel, G.F. de la Fuente, Bol. Soc. Esp. Ceram. **44**, 199 (2005)

10. G.F. de la Fuente, A. Sotelo, Y. Huang, M.T. Ruiz, A. Badia, L.A. Angurel, F. Lera, R. Navarro, C. Rillo, R. Ibanez, D. Beltran, F. Sapina, A. Beltran, Physica C **185**, 509 (1991)
11. L.D. Sykorova, O. Smrckova, V. Jakes, Phys. Status Solidi C **1**(7), 1952 (2004)
12. T. Kawai, T. Horiuchi, K. Mitsui, K. Ogura, S. Takagi, S. Kawai, Physica C **161**, 561 (1989)
13. V. Lennikov, B. Özkurt, L.A. Angurel, A. Sotelo, B. Özçelik, G.F. de la Fuente, J. Supercond, Nov. Magn. **26**, 947 (2013)
14. Y. Ando, A.N. Lavrov, S. Komiya, K. Segawa, X.F. Sun, Phys. Rev. Lett. **87**, 017001 (2001)
15. J.M. Tarascon, P. Barboux, G.W. Hull, R. Ramesh, L.H. Greene, M. Gariod, M.S. Hedge, W.R. Mckinnon, Phys. Rev. B **38**, 4316 (1989)
16. H. Eisaki, N. Kaneko, D. Feng, L. Fengi, A. Damascelli, P.K. Mang, Z.X. Shen, M. Greven, Phys. Rev. B **69**, 064512 (2004)
17. K. Fujita, T. Noda, K.M. Kojima, H. Eisaki, S. Uchida, Phys. Rev. Lett. **95**, 097006 (2005)
18. N. Knauf, J. Harwischmacher, R. Miiller, R. Borowski, B. Rodeu, D. Wohllebreu, Physica C **173**, 414 (1991)
19. C.J. Huang, T.Y. Tseng, T.S. Heh, F.H. Chen, W.S. Jong, Y.S. Fran, S.M. Shiau, Solid State Commun. **72**, 563 (1989)
20. A. Sotelo, G.F. De la Fuente, F. Lera, D. Beltran, F. Sapina, R. Ibanez, A. Beltran, M.R. Bermejo, Chem. Mater. **5**, 851 (1993)
21. H. Sözeri, N. Ghazanfari, H. Özkan, A. Kılıç, Supercod. Sci. Technol. **20**, 522 (2007)
22. D. Yazıcı, B. Özçelik, J. Supercond, Nov. Magn. **25**, 293–297 (2012)
23. B.D. Cullity, *Element of X-ray Diffraction* (Addison-Wesley Publishing Company Inc., Reading, 1956)
24. B. Özçelik, M. Gürsul, A. Sotelo, M.A. Maria, J. Mater. Sci.: Mater. Electron. **26**, 441–447 (2015)
25. O. Nane, B. Özçelik, J. Mater. Sci. **27**(7), 7633–7639 (2016)
26. C.P. Bean, Phys. Rev. Lett. **8**, 250 (1962)
27. D. Dew-Hughes, Philos. Mag. **30**, 293 (1974)

Publisher's Note Springer Nature remains neutral with regard to jurisdictional claims in published maps and institutional affiliations.